JOURNAL OF SYNCHROTRON RADIATION

ISSN 1600-5775

Simulations of Co-GISAXS during kinetic roughening of growth surfaces

Mahsa Mokhtarzadeh[a]* and Karl F. Ludwig Jr[b]

[a]Department of Physics, Boston University, Boston, MA 02215, USA, and [b]Division of Materials Science and Engineering, Boston University, Boston, MA 02215, USA. *Correspondence e-mail: mmokhtar@bu.edu

Received 19 February 2017
Accepted 16 August 2017

Edited by V. Favre-Nicolin, CEA and Université Joseph Fourier, France

Keywords: XPCS; Co-GISAXS; KPZ simulations; surface growth; correlation functions.

The recent development of surface growth studies using X-ray photon correlation spectroscopy in a grazing-incidence small-angle X-ray scattering (Co-GISAXS) geometry enables the investigation of dynamical processes during kinetic roughening in greater detail than was previously possible. In order to investigate the Co-GISAXS behavior expected from existing growth models, calculations and (2+1)-dimension simulations of linear Kuramoto–Sivashinsky and non-linear Kardar–Parisi–Zhang surface growth equations are presented which analyze the temporal correlation functions of the height–height structure factor. Calculations of the GISAXS intensity auto-correlation functions are also performed within the Born/distorted-wave Born approximation for comparison with the scaling behavior of the height–height structure factor and its correlation functions.

1. Introduction

The continued development of X-ray sources that can provide significant coherent flux has enabled the study of dynamics during a range of equilibrium and non-equilibrium processes. Using X-ray photon correlation spectroscopy (XPCS) (Shpyrko, 2014; Sutton, 2008; Sinha *et al.*, 2014) in a grazing-incidence small-angle X-ray scattering (Co-GISAXS) geometry offers extensive new opportunities to investigate surface dynamics on lateral length scales of 0.5 to 10^3 nm (Rainville *et al.*, 2015; Bikondoa *et al.*, 2013). In the steady-state regime of thin film growth where the ensemble averaged characteristics have reached saturation, the structure factor measured in a traditional time-resolved incoherent scattering experiment shows no further evolution; there is no ensemble averaged kinetics. However, local dynamical processes of deposition and relaxation continue and it is these that determine the final film structure. With the use of coherent X-rays, the auto-correlation function of the scattered light intensity $g_2(q, t)$ is accessible and reveals the underlying dynamics in the steady-state regime. In addition, to study the dynamics of the non-equilibrium system, two-time correlation functions $C(q, t_1, t_2)$ can be extracted from the Co-GISAXS experiments in the early time regime where the system is in a non-stationary phase.

Recent Co-GISAXS experiments have examined the thin film growth process of kinetic roughening which is often discussed through dynamical scaling relationships that connect spatial and temporal correlations and are independent of many system details. A key surface growth scaling relation is the Family Vicsek (Family & Vicsek, 1985; Vicsek & Family, 1984) scaling equation,

$$w(L, t) \simeq L^{\alpha} f(t/L^{z}), \qquad (1)$$

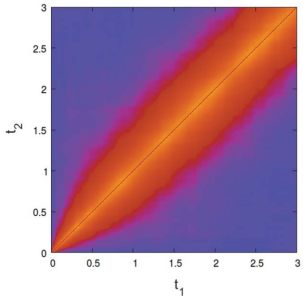

where $w(L, t)$ is the roughness of the interface or interface width, L is the lateral length scale, z is the dynamic growth exponent, α is the roughness exponent and $f(t/L^z)$ is a scaling function. This scaling relation describes behavior on length scales much larger than the lattice constant. For $u \rightarrow 1$, $f(u)$ behaves as a power law, $f(u) \rightarrow u^{\beta}$, and, for $u \rightarrow \infty$, the scaling function approaches a constant value so that $w(L, t) \simeq L^{\alpha}$. Therefore, the surface width approaches a steady-state value within the range of length scales studied. The cross-over time from power law growth to a constant roughness scales with lateral length scale: $t_x \simeq L^z$. Within the Family Vicsek scaling relation, when the evolution of the surface structure reaches a dynamical steady state the structure factor behaves as a power law, $S(q_{||}) \simeq q_{||}^{-m}$. Since the structure factor is directly proportional to the square of the interface width, m is related to α in d-dimensions as: $m = d + 2\alpha$ (Barabasi & Stanley, 1995). Moreover, the auto-correlation function of surface heights can be related to the dynamic exponent z in the steady state as (Sneppen *et al.*, 1992)

$$\langle h(q, t_1)\, h(q, t_2)\rangle \simeq F(q^z |t_1 - t_2|), \tag{2}$$

where F is a scaling function.

In XPCS experiments, the two-time correlation function is defined as

$$C(q, t_1, t_2) = \frac{\langle I(q, t_1)\, I(q, t_2)\rangle}{\langle I(q, t_1)\rangle \langle I(q, t_2)\rangle}, \tag{3}$$

where $I(q, t)$ is the intensity at wavevector q and time t and the angular brackets denote an ensemble average over equivalent q values.

In the dynamic steady state, it is useful to calculate the intensity auto-correlation function,

$$g_2(q, t) = \frac{\langle I(q, t')\, I(q, t' + t)\rangle}{\langle I(q, t')\rangle^2}. \tag{4}$$

The angular brackets indicate a time averaging over t' and equivalent q values. Often the experimental $g_2(q, t)$ functions are fit well with a Kohlrausch–Williams form (Kohlrausch, 1854),

$$g_2(q, t) = 1 + \beta(q) \exp\left\{-2[t/\tau(q)]^n\right\}, \tag{5}$$

where $\beta(q)$ is a contrast term with a value between zero and one that depends on the experimental setup and the coherence of the incident beam, and $\tau(q)$ is the q-dependent correlation time.

Comparing equation (5) with equation (2), we see that the correlation time $\tau(q)$ in the dynamic steady-state regime scales with the wavevector q ($q \simeq 2\pi/L$) as q^{-z}. Therefore, the dynamic scaling exponent z can be extracted directly from Co-GISAXS data under steady-state growth conditions.

Despite extensive theoretical and simulation studies on popular surface growth models, the intensity correlation functions that are now accessible through XPCS experiments have not been widely discussed in a manner that connects well to experiment. The XPCS correlation functions of two models specific to ion beam nano-patterning have been examined by Bikondoa *et al.* (2012). In contrast to that work, we focus here on models widely used to describe surface growth processes and investigate their analytical results and scaling behavior. Here, the height–height correlation functions are analyzed for both the (2+1)-dimensional linear Kuramoto–Sivashinsky (KS) (Kuramoto & Tsuzuki, 1975, 1976; Michelson & Sivashinsky, 1977; Sivashinsky, 1977; Halpin-Healy & Zhang, 1995) (§2) and the nonlinear Kardar–Parisi–Zhang (KPZ) (Barabasi & Stanley, 1995; Halpin-Healy & Zhang, 1995; Kardar *et al.*, 1986; Halpin-Healy & Takeuchi, 2015) (§3) growth models.

In §2 and §3 the correlations of the height–height structure factor $S(q)$ are examined. In the limit $q_z\sigma \ll 1$, where q_z is the component of the wavevector transfer perpendicular to the surface and σ is the root-mean-square (r.m.s.) surface roughness, the measured GISAXS signal is proportional to $S(q)$. Beyond this regime, where $q_z\sigma > 1$, the GISAXS intensity is not simply proportional to $S(q)$, but the simulations of §4 show that the intensity auto-correlation functions nonetheless yield accurate estimates of the surface growth scaling exponents except at low wavenumbers.

2. Linear theory

The linear growth model we examine is a model which considers random deposition of particles along with surface relaxation which leads to a correlated surface. We consider the linear KS model,

$$\frac{\partial h(\mathbf{r}, t)}{\partial t} = \nu\nabla^2 h - \kappa\nabla^4 h + \eta(\mathbf{r}, t), \tag{6}$$

where $h(\mathbf{r}, t)$ is the height of the interface, ν is proportional to the surface tension, κ is a positive parameter related to surface relaxation and $\eta(\mathbf{r}, t)$ is a Gaussian white noise with zero average, $\langle \eta(\mathbf{r}, t)\, \eta(\mathbf{r}', t)\rangle = 2D\delta(\mathbf{r} - \mathbf{r}')\, \delta(t - t')$.

The ensemble averaged height–height structure factor $S(q, t) = h(q, t)\, h^*(q, t)$ evolves as (Akcasu, 1989; Cook, 1970)

$$\begin{aligned}\langle S(q, t)\rangle = {} & \exp\left[-2\left(\nu q^2 + \kappa q^4\right)t\right] S_0(q) \\ & + \left[D/\left(\nu q^2 + \kappa q^4\right)\right]\left\{1 - \exp\left[-2\left(\nu q^2 + \kappa q^4\right)t\right]\right\},\end{aligned} \tag{7}$$

where S_0 comes from the initial condition at time zero. Therefore, the long-time steady-state behavior of $\langle S(q)\rangle$ is $\langle S(q, t \rightarrow \infty)\rangle = D/(\nu q^2 + \kappa q^4)$.

For the linear KS model, simulations were performed using the one-step Euler scheme in time for the temporal discretization. The spatial derivatives were calculated by the standard central finite difference discretization method on a square lattice of size $L = 1024$ with periodic boundary conditions. Taking advantage of the isotropy of the square lattice on long length scales, the values have been averaged over angle in reciprocal space and time after the system has reached a steady state. The simulations in Fig. 1 were performed with parameters $\nu = 1$, $\kappa = 30$, time step $dt = 10^{-3}$, number of iterations to reach steady state $N = 10^6$ and uniform random noise on the interval $[-1, 1]$. The results agree with the known $\langle S(q, t \rightarrow \infty)\rangle = D/(\nu q^2 + \kappa q^4)$ behavior, where q is the parallel momentum transfer $q = (q_x^2 + q_y^2)^{1/2}$. Fig. 1 shows that the cross-over regime for q^{-2} behavior at low q to q^{-4} behavior at high q is quite large. By tuning the relative coefficients

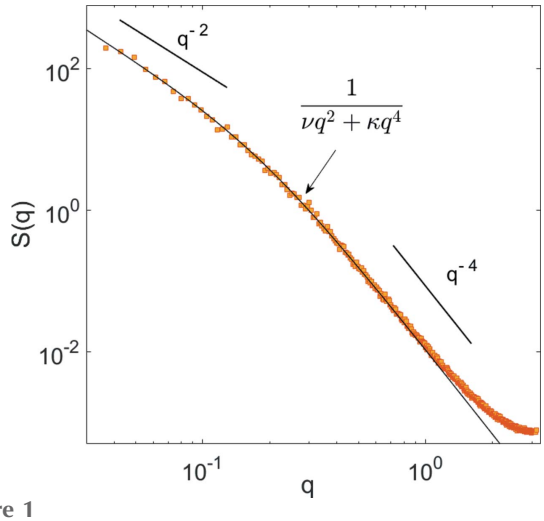

Figure 1
Steady-state structure factor for the linear KS model simulation with $L = 1024$, $\nu = 1$, $\kappa = 30$ and $dt = 10^{-3}$.

of ν and κ we can shift the scaling in a specific q range to either q^{-2}, q^{-4} or a value in between as the equation suggests: $1/(\nu q^2 + \kappa q^4)$. The upturn at high q is due to discrete lattice effects on short length scales.

2.1. Two-time correlation function

Following equation (3), we examine the two-time correlation function of the height–height structure factor,

$$C(q, t_1, t_2) = \frac{\langle S(q, t_1)\, S(q, t_2)\rangle}{\langle S(q, t_1)\rangle \langle S(q, t_2)\rangle}. \tag{8}$$

Taking the initial conditions to be: $S(q, t = 0) = h(q, t = 0)\, h^*(q, t = 0) = 0$, the structure factor becomes

$$\begin{aligned} S(q, t) = {} & \exp\left[-2\left(\nu q^2 + \kappa q^4\right)t\right] \\ & \times \int_0^t \int_0^t \exp\left[\left(\nu q^2 + \kappa q^4\right)(t' + t'')\right] \\ & \times \eta(q, t')\, \eta^*(q, t'')\, \mathrm{d}t'\, \mathrm{d}t''. \end{aligned} \tag{9}$$

Substituting (9) into (8) and calculating the value of the two-time correlation function, we obtain

$$C(q, t_1, t_2) = 1 + \frac{\exp\left[-2(\nu q^2 + \kappa q^4)(t_2 - t_1)\right] - \exp\left[-2(\nu q^2 + \kappa q^4)t_2\right]}{1 - \exp\left[-2(\nu q^2 + \kappa q^4)t_2\right]}. \tag{10}$$

Here we assume $t_2 > t_1$. Rewriting the above equation in terms of $T = t_1 + t_2$, $\Delta t = t_2 - t_1$ and the amplification factor $R(q) = (\nu q^2 + \kappa q^4)$ results in

$$C(q, T, |\Delta t|) = 1 + \frac{\exp[-2R(q)|\Delta t|] - \exp[-R(q)(T + |\Delta t|)]}{1 - \exp[-R(q)(T + |\Delta t|)]}, \tag{11}$$

which is valid for either $t_2 \geq t_1$ or $t_2 < t_1$. Fig. 2(*a*) shows the two-time correlation function simulated for a (2+1)-dimension linear model of lattice size $L = 1024$. The graph below in Fig. 2(*b*) is the diagonal cut of this function at different T values and the lines are the plotted function $C(|\Delta t|)$ in equation (11) with the specific values of T and $R(q)$ for $q \simeq 0.84$. As the graph shows, the width of the correlation function increases in the early period of growth and then saturates. The simulated values and the calculated theoretical function agree well with each other. Equation (11) shows that the characteristic time for saturation of the two-time correlation function width is $t_{\rm sat} \simeq 1/2R(q)$.

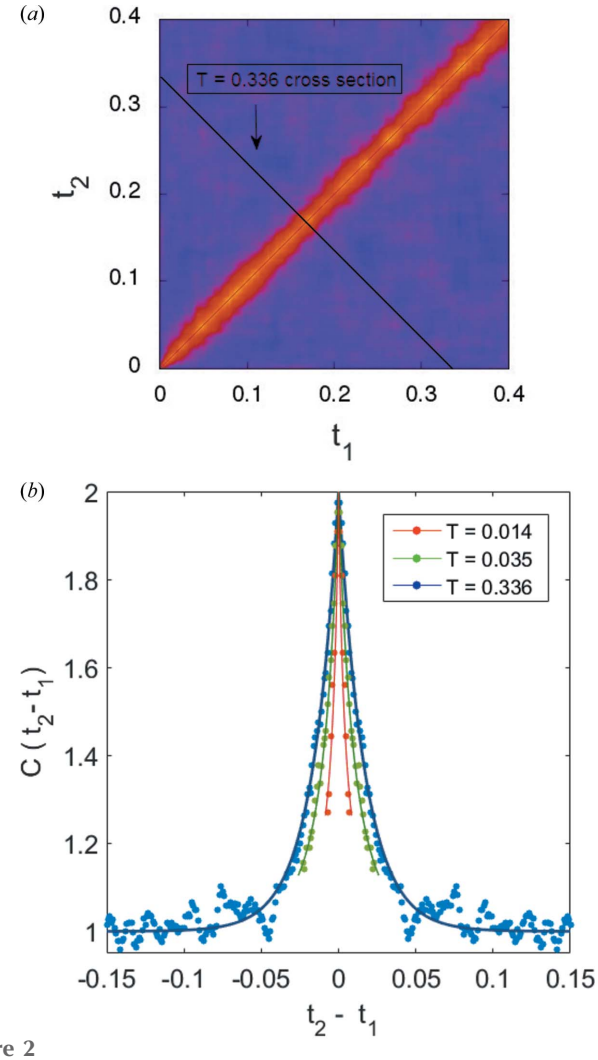

Figure 2
(*a*) Two-time correlation function $C(q, t_1, t_2)$ of the simulated intensity fluctuations for the linear KS model, $\nu = 1$, $\kappa = 58$, $dt = 5 \times 10^{-4}$, $L = 1024$ and $q = 0.84$. (*b*) The filled circles are the diagonal cut of the $C(q, t_1, t_2)$ function at different T values and the lines are the theoretical values calculated in equation (11).

2.2. Auto-correlation function

We next examine the structure factor auto-correlation function,

$$g_2(q, t) = \frac{\langle S(q, t')\, S(q, t' + t)\rangle}{\langle S(q, t')\rangle^2}, \tag{12}$$

where $S(q, t')$ is the structure factor at wavevector q and time t'. The angular brackets indicate a time averaging over t'.

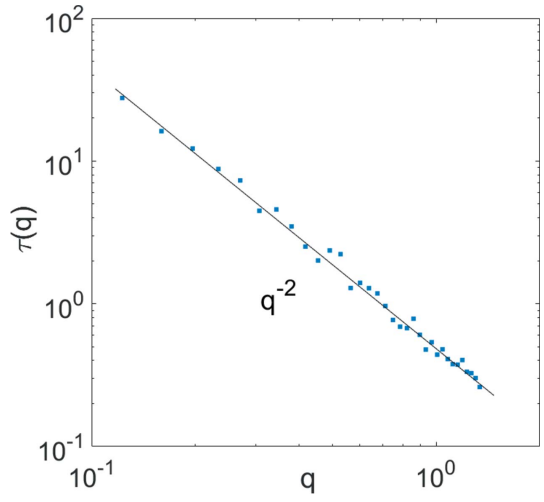

Figure 3
$\tau(q)$ for the linear model steady-state ($N = 3 \times 10^5$) simulation with L = 512, $\kappa = 0$, $\nu = 1$, $dt = 10^{-2}$. The solid line is a function proportional to $1/q^2$ predicted by the linear model.

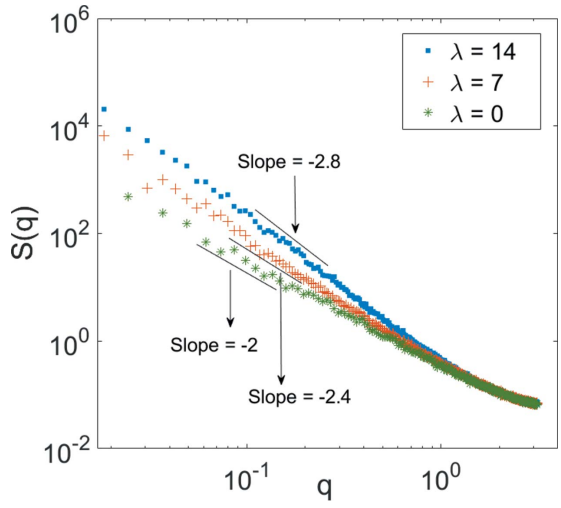

Figure 4
Late-stage structure factor for the KPZ model with increasing non-linear coefficients. Green: λ = 0 (linear model); red: λ = 7; blue: λ = 14, $\nu = 1$, lattice size L = 1024. For λ = 14, $dt = 10^{-3}$ and $N = 3 \times 10^6$ were used.

Analytical calculation shows that the above function at large t (steady-state) becomes

$$g_2(q, t) = 1 + \exp\left[-2\left(\nu q^2 + \kappa q^4\right)t\right]. \quad (13)$$

When the system has reached a steady state, the values start from $g_2(q, 0) = 2$ and relax to $g_2(q, t \to \infty) = 1$. Fitting the simulated correlation functions $g_2(q, t)$ for different q values with $g_2(t) = 1 + \exp[-(t/\tau)]$, we can find the fit parameter τ as a function of q. Fig. 3 shows the plotted correlation time $\tau(q)$ for the simple case of $\kappa = 0$. The solid line indicates the predicted $\tau(q) = 1/[2(\nu q^2 + \kappa q^4)]$ from equation (13). In this case, where $\kappa = 0$, the time constant is proportional to q^{-2}.

3. KPZ model

The KPZ equation (Kardar *et al.*, 1986) is one of the fundamental models for the study of non-equilibrium surface growth processes and scaling behavior. The non-linear stochastic partial differential equation which describes the evolution of the height function $h(\mathbf{r}, t)$ is written as follows,

$$\frac{\partial h(\mathbf{r}, t)}{\partial t} = \nu \nabla^2 h + (\lambda/2)|\nabla h|^2 + \eta(\mathbf{r}, t), \quad (14)$$

where λ corresponds to the effects of lateral growth. Galilean invariance, which is associated with the invariance of the KPZ equation under rotation of the coordinate system, yields the following relation for the growth exponents α and z: $\alpha + z = 2$ (Barabasi & Stanley, 1995; Tang, 1995). In (2+1)-dimensions, there are no exact results for α and z but various models have estimated the values to be approximately $\alpha \simeq 0.39$ and $z \simeq 1.6$ (Barabasi & Stanley, 1995; Kelling & Ódor, 2011). Numerical integration of the KPZ equation was carried out by choosing the standard finite difference discretization method for space derivatives along with one-step Euler time discretization. The results indicate that, for limited lattice sizes with periodic boundary conditions, the full KPZ behavior can be seen for sufficiently large non-linear coefficients. Considering the scaling behavior of the structure factor to be as q^{-m} with $m = 2\alpha + 2$, the linear model (λ = 0) gives the roughness exponent α to be zero as seen in Fig. 4: $S(q, t) \propto q^{-2}$. In the specific q range examined, the slope of the scaling function rises with increasing value of the non-linear coefficient, until it reaches its full KPZ scaling exponent of $2\alpha + 2 = 2.8 \to \alpha = 0.4$. Therefore, by tuning the non-linearity we can obtain a smooth transition from the linear regime to the strong non-linear regime in the observable q range of the simulation. The results below are in the strong coupling regime that gives the KPZ exponents.

3.1. Two-time correlation function

The two-time correlation function defined in equation (3) has been simulated for the KPZ model with parameters $\nu = 1$, λ = 14, $dt = 5 \times 10^{-3}$ and L = 1024. The results have been averaged over four realisations. Fig. 5 shows the two-time correlation function for $q = 0.92$. As the graph indicates, there is an increase in correlation times at the beginning of the growth process and then the correlation times saturate. We know of no analytical forms available for this process in order to compare with simulations. However, steady-state scaling behavior exists at late times and we address that with the auto-correlation function in the next section.

3.2. Auto-correlation function

In the KPZ model, the correlation function $g_2(q, t)$ does not show a simple exponential behavior. We take the fit functions to be of the form (Kohlrausch, 1854)

$$g_2(t) = 1 + \exp[-(t/\tau)^n]. \quad (15)$$

The simulations have been performed with coefficients $\nu = 1$, λ = 14, $dt = 10^{-3}$, $N = 3 \times 10^6$ and averaged over five realisations (Fig. 6). Fitting the $g_2(q, t)$ functions with

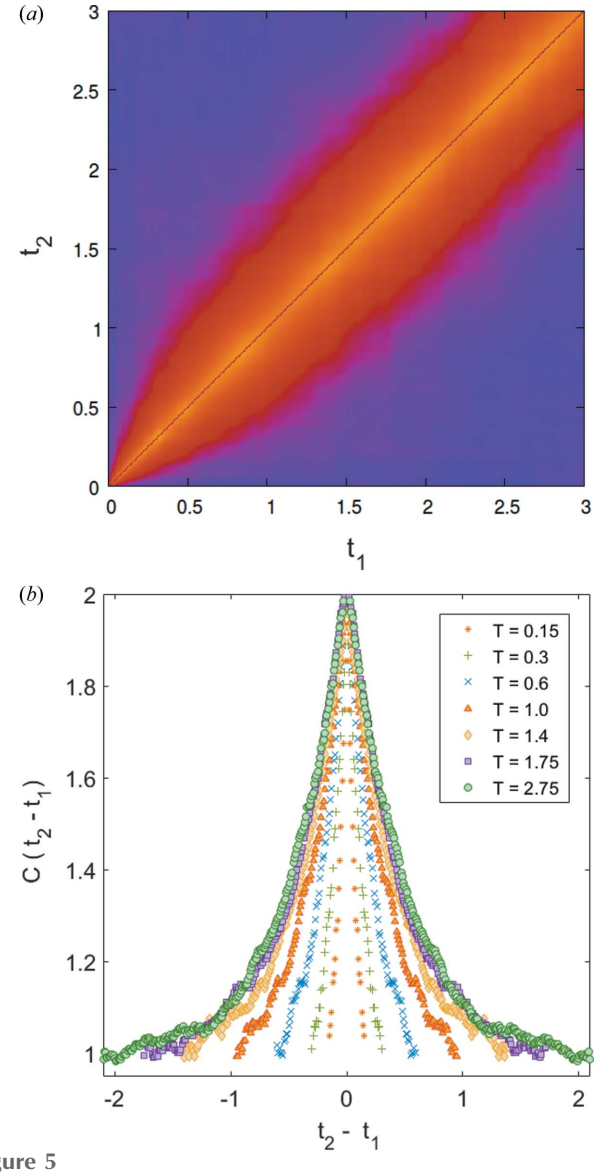

Figure 5
(*a*) Two-time correlation function $C(q, t_1, t_2)$ of the simulated intensity fluctuations for the KPZ model, $q = 0.92$. (*b*) The data are the diagonal cut of the $C(q, t_1, t_2)$ function at different T values.

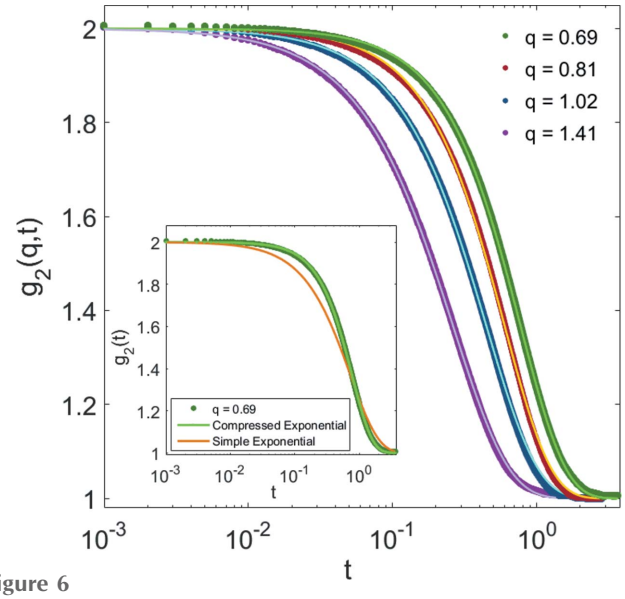

Figure 6
Late-stage auto-correlation functions $g_2(q, t)$ for the KPZ model, $L = 1024$, $\nu = 1$, $\lambda = 14$ and $dt = 10^{-3}$. The lines are the compressed exponential fits of the form in equation (15) to simulation data points. The inset displays the difference between a compressed and a simple exponential fit to $q = 69$.

equation (15), we find the values of the correlation times τ and exponents n for different q values. The $\tau(q)$ graph plotted in Fig. 7 scales as q^{-z}, where the dynamic exponent z is found to be: $z = 1.6$, consistent with known exponents for the (2+1)-dimensional KPZ model (Barabasi & Stanley, 1995; Kelling & Ódor, 2011). The exponent $n(q)$ plotted in Fig. 8 exhibits values greater than one, *i.e.* shows compressed exponential behavior. However, for high q, the KPZ $n(q)$ decreases towards one, indicative of simple exponential relaxation.

The compressed exponential behavior in the correlation functions results from the non-linearity of the KPZ equation. The relative effect of the non-linear term in the KPZ equation is larger for lower q values. This is seen by comparing the averaged magnitudes of the linear and non-linear terms for different q values and is plotted in Fig. 9. The inset displays the ratio of the non-linear to linear term in the KPZ equation. We have also performed numerical simulations of the restricted solid-on-solid stochastic deposition model (RSOS) (Kim & Kosterlitz, 1989; Kim *et al.*, 1991) since this model converges to a steady state very fast even for large lattice sizes and exhibits scaling behavior in accordance with the KPZ model. The growth algorithm for this model is to randomly select a site on a surface and to let the height of that site grow from h_i to $h_i + 1$ considering the restriction that the neighboring heights would differ by less than Δh at each step. In our simulations, we start with an initial configuration of a flat surface: $h_i = 0$, lattice size $L = 1024$ and consider periodic boundary conditions with maximum height difference of $\Delta h = 4$. As with the

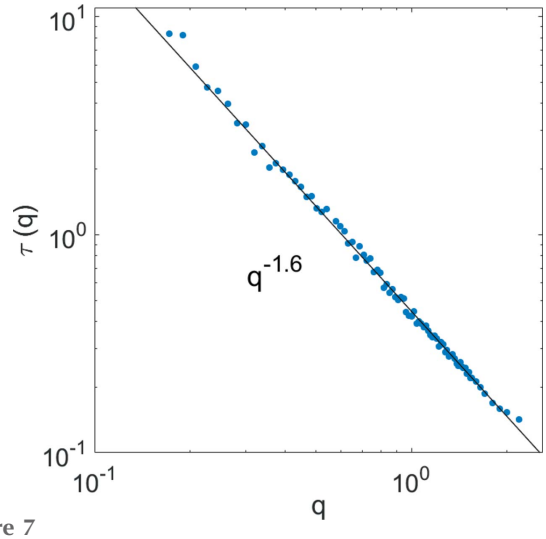

Figure 7
$\tau(q)$ derived from fitting the auto-correlation functions $g_2(q, t)$ to equation (15). The solid line is the function $f(q) = \text{constant} \times q^{-z}$, where z is the dynamic scaling exponent $z = 1.6$.

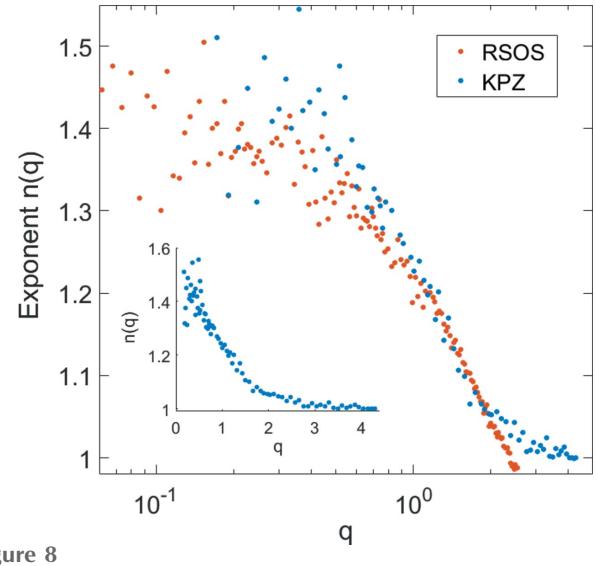

Figure 8
Compressed exponents $n(q)$ found from the KPZ and RSOS model simulations. These are determined by fitting the auto-correlation functions $g_2(q, t)$ to equation (15).

KPZ model, the correlation functions exhibit compressed exponential behavior; therefore, the same functional form as equation (15) is fitted to the data. The dynamic scaling exponent obtained from the correlation time $\tau(q)$ is found to be the same as the KPZ model, $z = 1.6$, and similarly the structure factor scales as $q^{-2.8} \rightarrow \alpha = 0.4$. The values of the compressed exponents $n(q)$ derived from this model in Fig. 8 are comparable with the KPZ values and they give exponents in the range 1.3–1.5 for the lowest measurable q values. While the RSOS model is in the same universality class as KPZ, it can be seen that its behavior at very high wavenumbers (short length scales) is different than that of the KPZ model. At these length scales, the discretization of the simulations likely

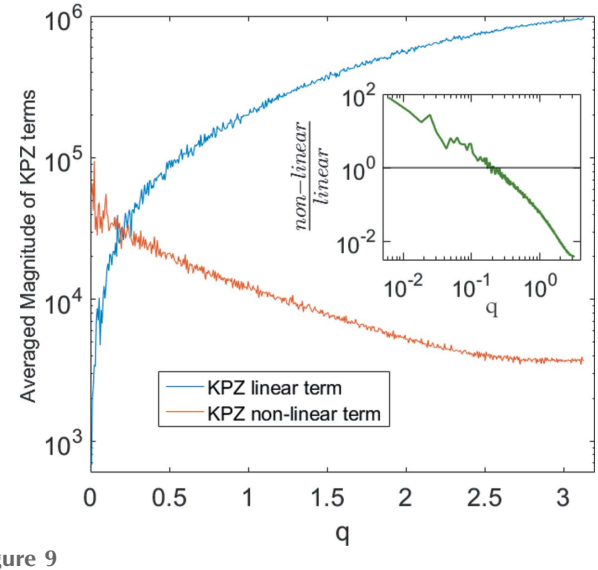

Figure 9
Average magnitude of the KPZ linear and non-linear terms plotted as a function of q for simulation values: $L = 1024$, $\nu = 1$, $\lambda = 14$, $dt = 10^{-3}$. The inset shows the average ratio of the non-linear term to the linear term.

becomes important. At the highest wavenumbers q, the discretization might also affect the relaxation process. However, comparison of Figs. 7 and 8 shows that $\tau(q)$ displays proper KPZ scaling even in the region where $n(q)$ is decreasing towards one.

4. Born/distorted-wave Born approximation

While §2 and §3 analyzed the correlation functions of the height–height structure factor $S(q)$, in general the measured GISAXS intensity $I(q)$ is not always proportional to $S(q)$. Within the Born approximation (BA), the measured GISAXS intensity from a surface of uniform density is (Sinha *et al.*, 1988)

$$I(q_x, q_y, q_z) \propto \left| \frac{1}{q_z} \iint \mathrm{d}x\, \mathrm{d}y \exp\left[-iq_z h(x, y)\right] \exp\left[-i\left(q_x x + q_y y\right)\right] \right|^2, \quad (16)$$

where q_z is the z-component of the wavevector change outside the material.

Higher-order multiple-scattering effects near the critical angle can necessitate the use of the distorted-wave Born approximation (DWBA) (Sinha *et al.*, 1988; Schiff, 1968; Vineyard, 1982; Rauscher *et al.*, 1995), which for a self-affine surface is (Sinha *et al.*, 1988)

$$I(q_x, q_y, q_z) \propto \left| \frac{1}{q_z^t} \iint \mathrm{d}x\, \mathrm{d}y \left\{ \exp\left[-iq_z^t h(x, y)\right] - 1 \right\} \times \exp\left[-i\left(q_x x + q_y y\right)\right] \right|^2, \quad (17)$$

where q_z^t is the z-component of the wavevector change inside the material.

Both the BA and DWBA expressions for the scattered intensity have the same form and the only difference is whether the z-component wavevector change is calculated outside or inside the material; this difference does not affect the simulation results.

Our aim is to investigate the robustness of scaling exponents obtained from correlations of the calculated GISAXS intensity rather than correlations of the structure factor itself. Using the form in equation (16), the intensity and the correlation functions were calculated for simulations of the (2+1)-dimension KPZ equation with $L = 1024$ and different values of $|q_z\sigma|^2$.

The results in Fig. 10 indicate that, even for values of $|q_z\sigma|^2 > 1$, the intensity differs from the $q^{-2.8}$ decay pattern only at low wavenumbers, as has been shown earlier by Salditt *et al.* (1995). The time constant $\tau(q)$ and compressed exponents $n(q)$ derived from the correlation functions are also independent of $|q_z\sigma|$ at high wavenumbers and they follow the same trend found in §3.

5. Conclusion

Analytical expressions for the auto-correlation and two-time correlation functions of the linear KS model have been

derived and confirmed here by simulation. For the non-linear KPZ model, the $g_2(t)$ auto-correlation function in the steady state is well fit by a compressed exponential function. The Siegert relation (Berne & Pecora, 1976) connects the intermediate scattering function $F(q, t)$,

$$F(q,t) = \frac{\langle h(q,t')\,h(q,t'+t)\rangle}{\langle h(q,t')\rangle^2}, \tag{18}$$

and the intensity auto-correlation function $g_2(q, t)$ as

$$g_2(q,t) = 1 + \left|F(q,t)\right|^2. \tag{19}$$

Thus the compressed exponential fit behavior of $g_2(q, t)$ implies that the intermediate scattering function also exhibits compressed exponential behavior in a similar time regime. This is consistent with theoretical results of Calaiori & Moore for the KPZ model (Colaiori & Moore, 2001*a*; Katzav & Schwartz, 2004) suggesting that at short time differences $F(q,t) \propto F_0(q,t)[1-(Bq^z t)^{m/z}]$, which is the expansion of a compressed exponential relaxation. Note that this is different from the stretched exponential (Colaiori & Moore, 2001*b*; Bustingorry, 2007) behavior found for large time differences t that were outside the scope of these simulations and, probably, beyond the scope of current XPCS measurements. The form of Calaiori & Moore predicts a compressed exponent in (2+1)-dimensions of $n = m/z = 1.75$ for small time differences. However, the fit compressed exponents measured here are q dependent and slightly smaller. It is possible that for larger lattices the exponent n can approach 1.75 at low wavenumbers.

Because the measured GISAXS intensity is not simply proportional to the height–height structure factor, we have also examined the auto-correlation function of the intensity as calculated within the BA/DWBA model. We have shown here that, beyond the $q_z\sigma \ll 1$ regime, the BA/DWBA expression for the diffuse scattering $I(q_x, q_y, q_z)$ gives valid scaling exponents at high wavenumbers. This shows that Co-GISAXS XPCS experiments can be clearly interpreted to give accurate information about the scaling dynamics of kinetic roughening.

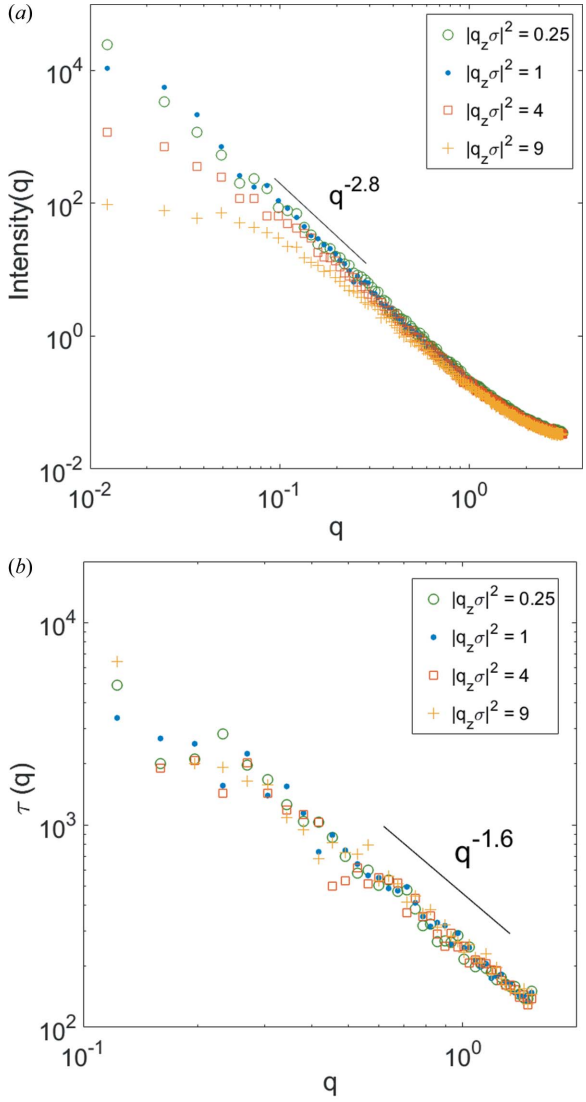

Figure 10
(*a*) Intensity and (*b*) correlation time constant $\tau(q)$ for BA simulations of the KPZ model for different values of $|q_z\sigma|^2$. Lattice size = 1024.

Acknowledgements

We thank Randall L Headrick for helpful discussions. We thank the manuscript reviewers for their valuable comments improving the paper.

Funding information

Funding for this research was provided by: NSF DMR-1307979.

References

Barabasi, A. L. & Stanley, H. E. (1995). *Fractal Concepts in Surface Growth*, p. 56 and p. 305. Cambridge University Press.
Berne, B. J. & Pecora, R. (1976). *Dynamic Light Scattering: With Applications in Chemistry, Biology and Physics.* New York: Wiley.
Bikondoa, O., Carbone, D., Chamard, V. & Metzger, T. (2012). *J. Phys. Condens. Matter*, **24**, 445006.
Bikondoa, O., Carbone, D., Chamard, V. & Metzger, T. H. (2013). *Sci. Rep.* **3**, 1850.
Bustingorry, S. (2007). *J. Stat. Mech.* **2007**, P10002.
Colaiori, F. & Moore, M. A. (2001*a*). *Phys. Rev. Lett.* **86**, 3946–3949.
Colaiori, F. & Moore, M. A. (2001*b*). *Phys. Rev. E*, **63**, 057103.
Cook, H. E. (1970). *Acta Metall.* **18**, 297–306.
Family, F. & Vicsek, T. (1985). *Physica A*, **18**, L75.
Halpin-Healy, T. & Takeuchi, K. A. (2015). *J. Stat. Phys.* **160**, 794–814.
Halpin-Healy, T. & Zhang, Y. C. (1995). *Phys. Rep.* **254**, 215–414.
Kardar, M., Parisi, G. & Zhang, Y. C. (1986). *Phys. Rev. Lett.* **56**, 889–892.
Katzav, E. & Schwartz, M. (2004). *Phys. Rev. E*, **69**, 052603.
Kelling, J. & Ódor, G. (2011). *Phys. Rev. E*, **84**, 061150.
Kim, J. M. & Kosterlitz, J. M. (1989). *Phys. Rev. Lett.* **62**, 2289–2292.
Kim, J. M., Kosterlitz, J. M. & Ala-Nissila, T. (1991). *J. Phys. A*, **24**, 5569–5586.
Kohlrausch, R. (1854). *Physik*, **167**, 179–214.
Kuramoto, Y. & Tsuzuki, T. (1975). *Prog. Theor. Phys.* **54**, 687–699.
Kuramoto, Y. & Tsuzuki, T. (1976). *Prog. Theor. Phys.* **55**, 356–369.
Michelson, D. M. & Sivashinsky, G. I. (1977). *Acta Astronaut.* **4**, 1207–1221.

Rainville, M. G., Wagenbach, C., Ulbrandt, J. G., Narayanan, S., Sandy, A. R., Zhou, H., Headrick, R. L. & Ludwig, K. F. (2015). *Phys. Rev. B*, **92**, 214102.
Rauscher, M., Salditt, T. & Spohn, H. (1995). *Phys. Rev. B*, **52**, 16855–16863.
Salditt, T., Metzger, T. H., Brandt, Ch., Klemradt, U. & Peisl, J. (1995). *Phys. Rev. B*, **51**, 5617–5627.
Schiff, S. I. (1968). *Quantum Mechanics.* New York: McGraw-Hill.
Shpyrko, O. G. (2014). *J. Synchrotron Rad.* **21**, 1057–1064.
Sinha, S. K., Jiang, Z. & Lurio, L. B. (2014). *Adv. Mater.* **26**, 7764–7785.
Sinha, S. K., Sirota, E. B., Garoff, S. & Stanley, H. B. (1988). *Phys. Rev. B*, **38**, 2297–2311.
Sivashinsky, G. I. (1977). *Acta Astronaut.* **4**, 1177–1206.
Sneppen, K., Krug, J., Jensen, M. H., Jayaprakash, C. & Bohr, T. (1992). *Phys. Rev. A*, **46**, R7351–R7354.
Sutton, M. (2008). *C. R. Phys.* **9**, 657–667.
Tang, L.-H. (1995). *Annual Reviews of Computational Physics II*, edited by D. Stauffer, p. 143. Singapore: World Scientific.
Vicsek, T. & Family, F. (1984). *Phys. Rev. Lett.* **52**, 1669–1672.
Vineyard, G. H. (1982). *Phys. Rev. B*, **26**, 4146–4159.
Ziya Akcasu, A. (1989). *Macromolecules*, **22**, 3682–3689.